

# Underwater acoustic spiral source: pool tests and calibration

Rúben Viegas\*, Friedrich Zabel<sup>†</sup> and António J. Silva<sup>‡</sup>

\*LARSyS, Universidade do Algarve, Campus de Gambelas, 8005-139 Faro, Portugal

Email: a77916@ualg.pt

<sup>†</sup>CINTAL, Universidade do Algarve, Campus de Gambelas, 8005-139 Faro, Portugal

Email: fredz@ualg.pt

<sup>‡</sup>LARSyS, Universidade do Algarve, Campus de Gambelas, 8005-139 Faro, Portugal

Email: asilva@ualg.pt

**Abstract**—Underwater acoustic spiral sources are able to generate spiral acoustic fields where the phase depends on the bearing angle. It allows to estimate the bearing angle relatively to a receiver by subtracting the phases of a spiral and a circular wavefront, and can be used to estimate bearing angles with a single hydrophone/projector pair, e.g., for unmanned underwater vehicles localization. The developed spiral source comprises four monopoles/quadrants and it will be shown that the spiral source behavior is linear, which means that the generated acoustic signals are the sum of the four acoustic signals from each separate monopole, for any amplitude value. This work presents two calibration methods for spiral acoustic sources and the linearity evaluation for the used spiral source. Unlike the calibrations performed on signal reception, the two proposed calibration methods adjust the phase of the emitted signals to form the acoustic spiral field. The first calibration method rectifies the phase of one quadrant based on the contribution of the four quadrants. This method was tested and presented a performance lower than the performance of the calibration on the receiving side. After evaluating the linearity, a new calibration approach is suggested. This new approach uses the signals from separate quadrants instead of the contribution of the four quadrants. This method needs to be tested experimentally to check its validity.

**Index Terms**—Spiral Source, Underwater Acoustics, Transducer Calibration, Underwater Localization

## I. INTRODUCTION

In the last 10 years, the use of spiral acoustic fields have emerged as promising solutions for underwater localization [1], [2] and target detection SONAR [3]. The spiral acoustic fields can be generated using two different spiral source approaches [4]: vibrating a spiral-shaped surface, termed as “Physical-Spiral”; and vibrating multiple acoustic elements with different phases, termed as “Phased-Spiral”. The physical-spiral sources have the disadvantage of being inherently narrowband unlike the phased-spiral sources [4]. Over the years, some spiral source designs have been developed, with both physical [5] and phased [5]–[9] approaches.

Underwater localization using spiral acoustic fields consists of emitting a circular wavefront and a spiral wavefront, allowing a receiver to compute the direction to the source by subtracting the phases of the two wavefronts. The circular wavefront propagates with a constant phase at any direction, while in the spiral wavefront the phase varies linearly with the bearing angle relative to the acoustic source. This system

has the advantage of only needing a single source/hydrophone pair to determine the direction (azimuth or altitude, depending on the spiral source orientation) based on the phases, without time-of-flight (ToF) dependency [2], and without requiring the use of an array of hydrophones. The distance between the source and the receiver can be obtained using the ToF.

More recently, a new spiral source approach was presented which is based on four omnidirectional monopoles [10]. The spiral source’s prototype was made using a standard PZT-4 piezoelectric ceramic hollow cylinder with four inner and outer ribs on the conductive layer, forming the four quadrants shown in Figure 1. With the four monopoles driven with the same signal it is possible to generate a circular acoustic field and with the four monopoles driven with quadrature signals it is possible to generate a spiral acoustic field.

In [10] is presented a phase calibration that performs phase adjustments after the signal reception, based on the data from previous recordings. This calibration method, from now on referred to as Method 0, presented absolute angle errors of less than  $2.5^\circ$  above 50 kHz, and less than  $11^\circ$  below 50 kHz. In this work, two new calibration methods are proposed. Both methods are performed by adjusting the emitted signals, to generate the spiral acoustic fields with the intended shapes. All experiments were performed with the spiral source described in [10].

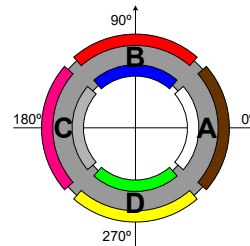


Fig. 1: Spiral Source quadrants A, B, C and D: grey is the piezoceramic material, and the other colors are the electrodes.

In section II, the experimental setup is described. In section III, the Method 1 for the spiral source calibration is presented and the results are compared with the reception calibration

method presented in [10]. In section IV, the spiral source linearity is experimentally confirmed and is used in section V to develop the Method 2 for the spiral source calibration. In section VI, the conclusion and future work are presented.

## II. EXPERIMENTAL SETUP

The laboratory acoustic experiments reported in this work were carried in January 2023 in a water tank at the Robotics and Autonomous Systems (CRAS), at FEUP, Porto, Portugal. The physical setup was the same as described in [10]. Figure 2, shows the underwater experimental setup with the spiral source in the middle, on the left the receiving hydrophone RESON TC4032, on the right the hydrophone RESON TC4033, the black arrows represent the relevant dimensions, and the colored arrows represent the direct, surface reflected and bottom reflected paths. In this work only signals from the hydrophone TC4033 will be analyzed. The spiral source was placed at 0.84 m depth, at 0.88 m from the bottom, and the hydrophone was placed at the spiral source depth, at a horizontal distance of 1 m.

As in [10], a sequences of chirps, with duration of 0.8 ms and a frequency increase of 500 Hz, with initial frequencies from 20 kHz to 75 kHz, with a step of 5 kHz, were emitted. Figure 3 shows the signal sequence emitted in the four quadrants of the spiral source for multiple frequency analysis: the white blocks represent pauses, the gray blocks represent the chirps for generating circular wavefronts, and the chirps with the other four colors represent the phase-shifted chirps for generating spiral wavefronts.

The transmitted chirps for the circular wavefront are given by

$$r_q(t) = \sin\left(2\pi\left(\frac{f_1 - f_0}{2\Delta t}t^2 + f_0 t\right)\right), \quad (1)$$

where  $q \in \{A; B; C; D\}$ ,  $f_0$  and  $f_1$  are the start and end frequencies, respectively, and  $\Delta t$  is the chirp duration. The transmitted chirps for the spiral wavefront are given by

$$s_q(t) = \sin\left(\phi_q + 2\pi\left(\frac{f_1 - f_0}{2\Delta t}t^2 + f_0 t\right)\right), \quad (2)$$

where  $\phi_q$  is the initial phase of each quadrant. The applied  $\phi_q$  values were  $\phi_A = 0^\circ$ ,  $\phi_B = 90^\circ$ ,  $\phi_C = 180^\circ$ , and  $\phi_D = 270^\circ$ .

After the chirp transmission, the signals are acquired at the hydrophone output and the direct paths of the acoustic signals are extracted using the cross-correlation method described in [10]. The direct path signal due to the circular wavefront and the one due to the spiral wavefront will be termed  $r(t)$  and  $s(t)$ , respectively. The phase difference between the two signals (reference and spiral) is given by

$$\Delta\phi(f_i, \theta) = B[\arg(S(f_i)) - \arg(R(f_i))], \quad (3)$$

where  $R(f)$  and  $S(f)$  are the Fourier transforms of the received  $r(t)$  and  $s(t)$  signals, respectively,  $B[\cdot]$  is a bounding operation that bounds the angle in the range  $[-\pi; \pi]$ ,  $\arg(\cdot)$  is the complex argument function, and  $\theta$  is the spiral source bearing angle relatively to the hydrophone.

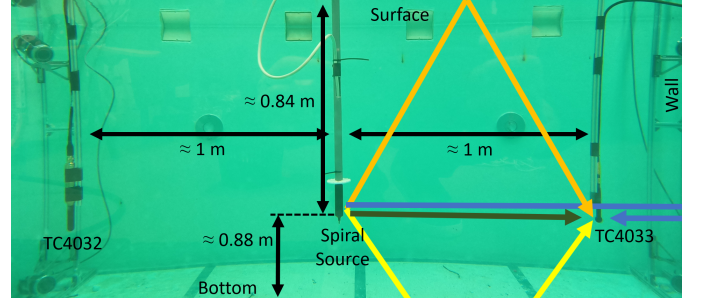


Fig. 2: Underwater experiment setup with the Spiral Source (in the center), and the hydrophones TC4033 and TC4032. The color arrows show the underwater acoustic paths illustrated for the hydrophone TC4033: direct path (dark green), path with one surface reflection (orange), path with one bottom reflection (yellow), and path with one wall reflection (blue).

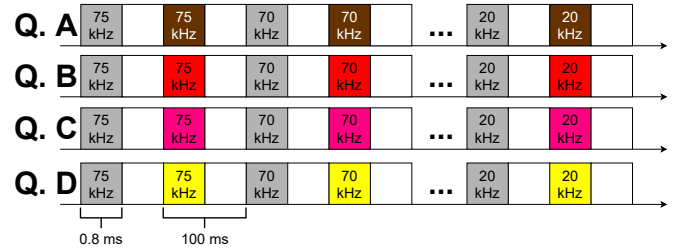


Fig. 3: The signal sequence emitted in the four quadrants of the spiral source ("Q. A", "Q. B", "Q. C", and "Q. D") for multiple frequency analysis: the white blocks represent pauses, the gray blocks represent the chirps for generating circular wavefronts, and the chirps with the other four colors represent the phase-shifted chirps for generating spiral wavefronts.

## III. PHASE CALIBRATION: METHOD 1

The proposed phase calibration methods consists of maintaining the same phase values for the emission of the circular wavefront, and apply different frequency-dependent phases for the emitted chirps for the spiral wavefront.

In method 1, signals were acquired in the four positions of the spiral source corresponding to each of the quadrants:  $\theta_A = 0^\circ$ ,  $\theta_B = 90^\circ$ ,  $\theta_C = 180^\circ$ , and  $\theta_D = 270^\circ$ . The phase systematic errors are bearing angle,  $\theta$ , and frequency,  $f_i$ , dependent, thus resulting that  $\Delta\phi^{M1}(f_i, \theta)$  is given by [10]

$$\Delta\phi^{M1}(f_i, \theta) = \theta + \varepsilon^{M1}(f_i, \theta), \quad (4)$$

where  $\varepsilon^{M1}(f, \theta)$  is the phase systematic error, and can be determined if the "measured"  $\Delta\phi(f_i, \theta)$  and the "true"  $\theta$  are known. Since it is intended to remove the systematic errors, the new phase values of each quadrant are given by

$$\phi_q^{M1}(f_i) = \phi_q - \varepsilon^{M1}(f_i, \theta_q). \quad (5)$$

Consequently, based on the phase differences obtained with (3), the frequency-dependent phases for the emitted chirps for the spiral wavefront  $\phi_q^{M1}(f)$  are calculated using the following expression

$$\phi_q^{M1}(f_i) = \phi_q + \theta_q - \Delta\phi^{M1}(f_i, \theta_q). \quad (6)$$

Figure 4 shows the measured phase difference with (3) and the calculated calibrations values  $\phi_q^{M1}(f)$ , for each study frequency  $f_i$ , for each quadrant. It is possible to observe that the adjustment values in Fig. 4b vary considerably with frequency, feature that was also observed in [10] which is due to the strong phase difference variation along the frequency observed in Fig. 4a.

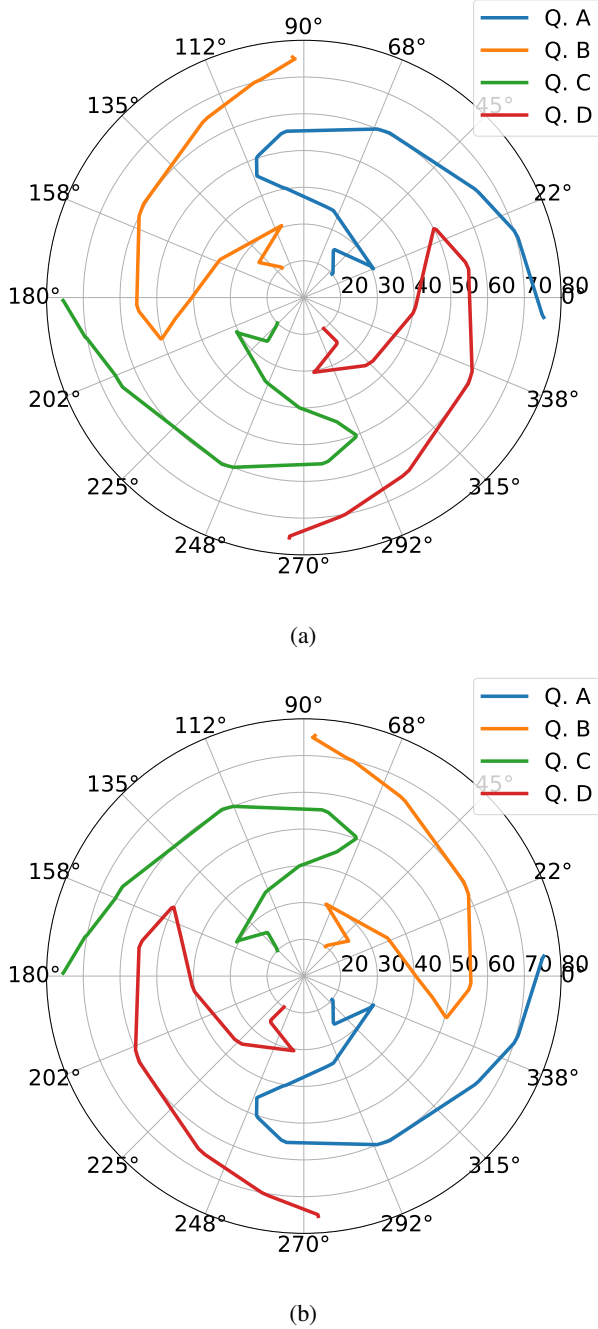


Fig. 4: Measured phase difference (a) and the calculated calibrations values (b), along frequency, for each quadrant of the spiral source.

Then, the transmitted chirps for the spiral wavefront were

generated with (2) with  $\phi_q^{M1}(f)$  values instead of  $\phi_q$  values. The signals were emitted and the respective acoustic signals were recorded in 16 different positions of the spiral source. Figure 5 shows the calculated phase differences, along frequency  $f$ , for the adjusted phases of the emitted chirps  $\phi_q^{M1}(f)$ , at multiple positions  $\theta$ . It also shows the results of Method 0 in the dashed lines, under the same conditions. The Figure 5 shows that the phase difference values from the two methods correspond approximately to the position of the acquisition, but there are still angular errors. This calibration method presented maximum absolute angle errors of less than  $15^\circ$  above 50 kHz, and less than  $35^\circ$  below 50 kHz. Between 35 and 45 kHz it is possible to observe a high variability of values. Thus, the maximum absolute errors of method 1 are much greater than the maximum absolute errors of method 0 ( $2.5^\circ$  above 50 kHz, and less than  $11^\circ$  below 50 kHz). The performance difference between the two methods can be observed in Fig. 5.

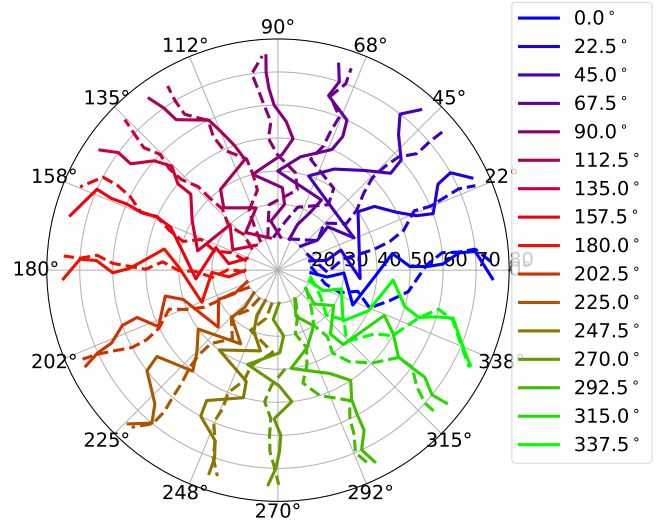


Fig. 5: Calculated phase differences along frequency at 16 positions using Methods 0 and 1. The dashed lines correspond to method 0 values and the solid lines correspond to method 1 values.

After analyzing the results, it was concluded that it is not accurate to rectify the phase of one quadrant based on the contribution of the four quadrants. One way to improve the presented calibration method is to evaluate the phase of the quadrants separately, and for that the system of the four quadrants should be linear.

#### IV. LINEARITY EVALUATION

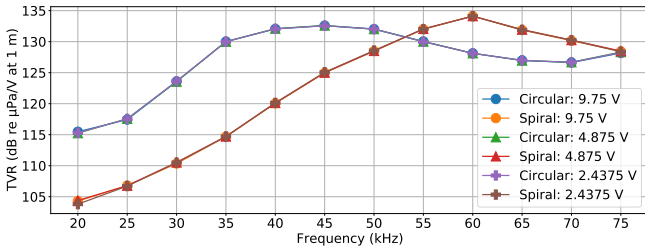
The linearity evaluation aimed to test whether the quadrants of the spiral source are in accordance with the equation

$$\mathbf{T} \left( \sum_{q=A}^D \alpha_q x_q(t) \right) \stackrel{?}{=} \sum_{q=A}^D \alpha_q \mathbf{T}(x_q(t)), \quad (7)$$

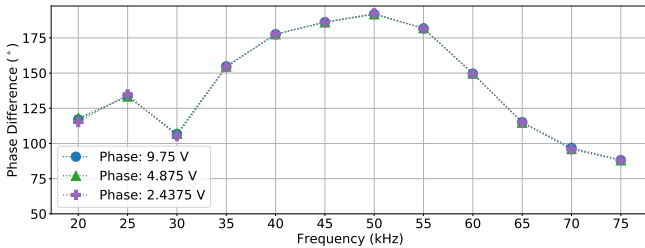
where  $T()$  is the transformation of the emitted signals,  $\alpha_q$  is a multiplicative constant for quadrant  $q$ , and  $x_q(t)$  is the signal emitted in quadrant  $q$ . For a system to be linear, i. e., that the emission of the four quadrants simultaneously is equal to the sum of the emission of the quadrant frames separately, the system must be homogeneous and additive.

To test the homogeneity, three acquisitions were performed with input signals with different amplitudes: 9.75 V, 4.875 V and 2.4375 V. From the three acquisitions were calculated: (i) the Transmitting Voltage Response (TVR) values for the two types of wavefront (circular and spiral); and (ii) the phase difference between the two wavefronts. Figures 6a and 6b show the TVR values and the phase differences, respectively. It is possible to state that, as the TVR values and the phase differences are very similar for different amplitudes since the curves almost overlap, and so the TVR and the phase of the spiral source does not depend on the amplitude of the signal. Thus, it is possible to consider that the spiral source is a homogeneous system.

To test the additivity, the sequence of the transmitted signals needed to be changed. Figure 7 shows the signal sequence emitted in the four quadrants of the spiral source for the additivity test. The sequence starts with the emission of a circular wavefront, followed by a spiral wavefront (in the following termed as simultaneous signals, because all four quadrants are driven at the same time); and then the circular and spiral signals of each quadrant are emitted separately (in the following termed as separate signals, because only one quadrant is driven at a time).



(a)



(b)

Fig. 6: Homogeneity test: (a) TVR and (b) phase difference values measured using the TC4033 hydrophone, for emitting amplitudes of 9.75 V, 4.875 V, and 2.4375 V.

After isolating the direct paths of the ten received signals, the signals from each quadrant are summed and compared

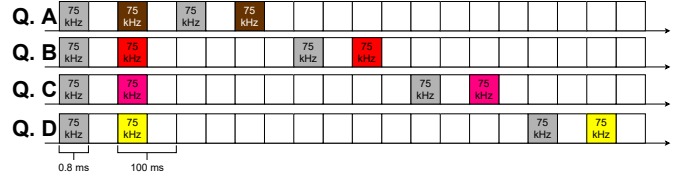


Fig. 7: The signal sequence emitted in the four quadrants of the spiral source ("Q. A", "Q. B", "Q. C", and "Q. D") for the additivity test: the white blocks represent pauses, the gray blocks represent the chirps for generating circular wavefronts, and the chirps with the other four colors represent the phase-shifted chirps for generating spiral wavefronts.

with the simultaneous signal. This process was done for the circular wavefront and for the spiral wavefront. The signal resultant from the sum of the four signals from each quadrant, from now on, is termed separate signal. Figure 8 shows an example of the additivity test for 70 kHz. In both wavefront types, the signals have identical amplitudes and phases, so it is possible to state that the spiral source looks additive, at least, for 70 kHz.

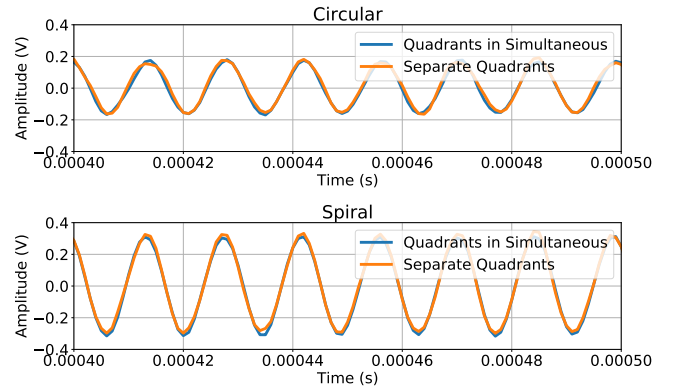


Fig. 8: Example of the additivity test for 70 kHz, for the circular wavefront (on top) and for the spiral wavefront (at bottom).

In order to compare the amplitude and phase of the two signals (simultaneous and separate), two metrics were used to evaluate the additivity of the spiral source along the frequency, in four different positions: Relative Error Percentage of Amplitude, and Absolute Phase Difference. The first metric is given by the equation

$$\varepsilon_A = \frac{100 \cdot |A_{\text{simul}} - A_{\text{sep}}|}{A_{\text{simul}}}, \quad (8)$$

where  $A_{\text{simul}}$  and  $A_{\text{sep}}$  are the amplitudes of the simultaneous and separate signals, respectively, that were obtained from the Fourier transform of the signals. The Absolute Phase Difference is the absolute value of (3).

Figure 9 shows the Relative Error Percentage of Amplitude, and Phase Difference, between: the circular or spiral wavefront; and the sum of the signals from each quadrant. The

four subfigures 9a, 9b, 9c, and 9d represent the obtained results with each spiral source quadrant pointed to the hydrophone, which corresponds to the positions  $0^\circ$ ,  $90^\circ$ ,  $180^\circ$ , and  $270^\circ$ , respectively. The results presented in the figures shows that the Relative Error Percentage of Amplitude, and Phase Difference are always less than 6% and  $4^\circ$ , respectively, and that the values are smaller between 40 kHz and 65 kHz.

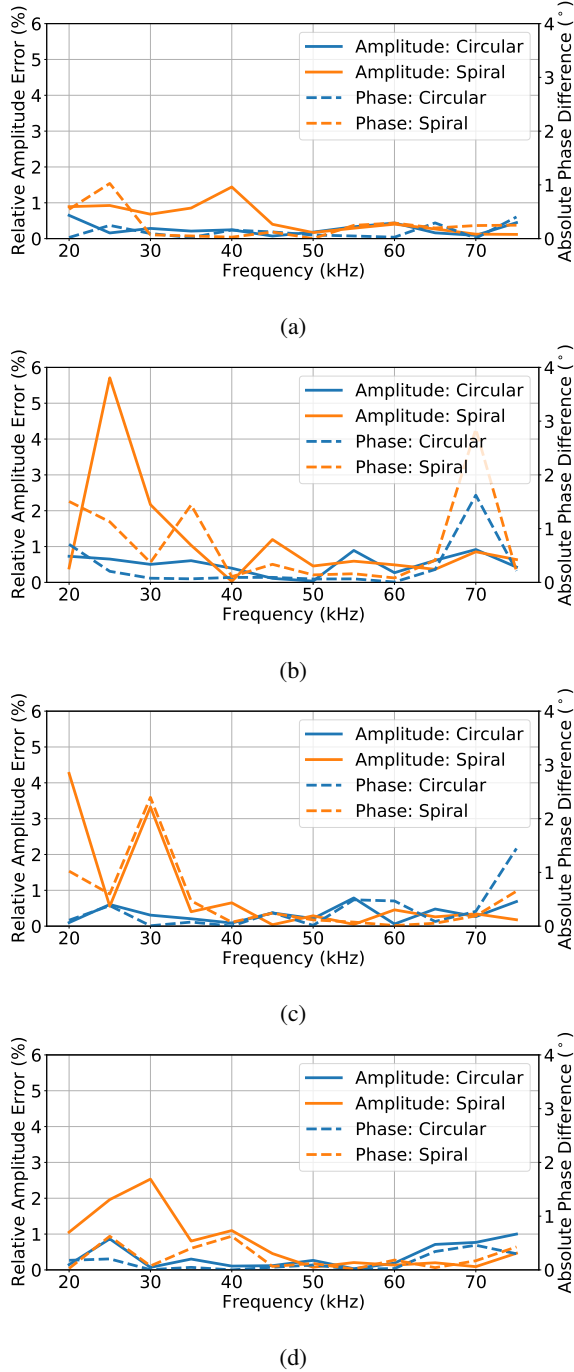


Fig. 9: Relative Error Percentage of Amplitude, and Phase Difference, between: the circular or spiral wavefront; and the sum of the signals from each quadrant. The data were acquired at the positions (a)  $0^\circ$ , (b)  $90^\circ$ , (c)  $180^\circ$ , and (d)  $270^\circ$ .

Since the results show amplitude and phase errors lower than 6% and  $4^\circ$ , respectively, it is possible to state that the simultaneous signals are approximately equal to the separate signals, and consequently, that the spiral source is additive. Therefore, since it is also homogeneous, the developed spiral source can be considered a linear system.

## V. PHASE CALIBRATION: METHOD 2

Considering that the spiral source is linear, a different methodology for phase calibration can be developed, which corresponds to adjusting the phase transmitted from each quadrant based on the phase difference between the circular wavefront and the acoustic signal generated in each quadrant separately. The required adjusting phases can be extracted from the recordings with the sequence from Figure 7. This proposed calibration method is termed Method 2.

The phase difference between the circular wavefront signal and a separate signal is given by

$$\Delta\phi^{M2}(f_i, \theta) = \varepsilon^{M2}(f_i, \theta), \quad (9)$$

where  $\varepsilon^{M2}(f, \theta)$  is the phase systematic error. Since it is intended to remove the systematic errors, the new phase values for the signals to be transmitted in each quadrant are given by

$$\phi_q^{M2}(f_i) = \phi_q - \varepsilon^{M2}(f_i, \theta_q). \quad (10)$$

The emission of the signals from (2) with the suggested phases  $\phi_q^{M2}(f)$  instead of  $\phi_q$  must be tested experimentally to confirm the validity of the proposed method 2 for the spiral source calibration.

## VI. CONCLUSION

Underwater localization and navigation using spiral acoustic sources has shown to be a promising solution. In this work, two different calibrations of spiral sources are presented: Method 1 and 2. The first proposed calibration method was tested and showed acceptable results. On the other hand, it performs worse than the calibration performed on signal reception described in [10]. Then, from the homogeneity and additivity tests, it was considered that the developed spiral source is linear, and in order to improve the calibration results, a new calibration methodology for linear spiral sources was proposed (Method 2).

In future works, an accurate spiral source bearing angle positioning system should be used for better calibration tests, including for the demonstration of the method 2. An accurate calibration methodology will lead to an improvement in systems using spiral sources.

## VII. ACKNOWLEDGEMENT

We would like to thank Dr. Nuno Cruz from Robotics and Autonomous Systems (CRAS) at FEUP, Porto, Portugal for the invitation to carry out the acoustic experiments at the CRAS's water tank facilities. This work was supported by the project K2D: Knowledge and Data from the Deep to Space with reference POCI-01-0247-FEDER-045941, cofinanced by the European Regional Development Fund (ERDF), through

the Operational Program for Competitiveness and Internationalization (COMPETE2020), and by the Portuguese Foundation for Science and Technology (FCT) under the MIT Portugal Program.

#### REFERENCES

- [1] B. R. Dzikowicz, B. T. Hefner, and R. A. Leasko, "Underwater acoustic navigation using a beacon with a spiral wave front," *IEEE Journal of Oceanic Engineering*, vol. 40, no. 1, pp. 177–186, 1 2015.
- [2] B. R. Dzikowicz, J. Y. Yoritomo, J. T. Heddings, B. T. Hefner, D. A. Brown, and C. L. Bachand, "Demonstration of spiral wavefront navigation on an unmanned underwater vehicle," *IEEE Journal of Oceanic Engineering*, pp. 1–10, 2023.
- [3] B. R. Dzikowicz, J. F. Tressler, and D. A. Brown, "Demonstration of spiral wave front sonar for active localization," *The Journal of the Acoustical Society of America*, vol. 146, no. 6, pp. 4821–4830, 12 2019.
- [4] B. T. Hefner and B. R. Dzikowicz, "A spiral wave front beacon for underwater navigation: Basic concept and modeling," *The Journal of the Acoustical Society of America*, vol. 129, no. 6, pp. 3630–3639, 6 2011.
- [5] B. R. Dzikowicz and B. T. Hefner, "A spiral wave front beacon for underwater navigation: Transducer prototypes and testing," *The Journal of the Acoustical Society of America*, vol. 131, no. 5, pp. 3748–3754, 5 2012.
- [6] D. A. Brown, B. Aronov, and C. Bachand, "Cylindrical transducer for producing an acoustic spiral wave for underwater navigation (I)," *The Journal of the Acoustical Society of America*, vol. 132, no. 6, pp. 3611–3613, 12 2012.
- [7] D. Brown, C. Bachand, and B. Aronov, "Design, development and testing of transducers for creating spiral waves for underwater navigation," in *Meetings on Acoustics*. ASA, 2013.
- [8] W. Lu, Y. Lan, R. Guo, Q. Zhang, S. Li, and T. Zhou, "Spiral sound wave transducer based on the longitudinal vibration," *Sensors*, vol. 18, no. 11, p. 3674, 10 2018.
- [9] W. Lu, R. Guo, Y. Lan, H. Sun, S. Li, and T. Zhou, "Underwater spiral wave sound source based on phased array with three transducers," *Sensors*, vol. 19, no. 14, p. 3192, 7 2019.
- [10] R. Viegas, F. Zabel, and A. Silva, "In lab demonstration of an underwater acoustic spiral source," *Preprints.org*, no. 2023040272, 2023.